

NUMERICAL ANALYSIS OF THE SHAPE EFFECT ON THE TENSILE STRENGTH EVALUATION OF AXISYMMETRIC SPECIMENS

L. C. ZHANG

Department of Mechanics, Zhejiang University, Hangzhou 310027, People's Republic of China

SUMMARY

This paper analyses the shape effect on the tensile strength of axisymmetric rock specimens by an improved adaptive dynamic relaxation method. It is shown that the present approach is convenient and efficient. Numerical results for spheroidal specimens with different shapes reveal the variation of stress distributions along the loading axes and suggest that loading along the shorter principal axis is preferable in strength tests. Furthermore, an empirical formula based on the failure criterion of maximum tensile stress is proposed to evaluate the tensile strength of specimen materials.

1. INTRODUCTION

It is known that the failure of brittle materials such as rock and concrete shows definite characteristics of tensile break under a pair of compressive point loads. As early as the 1930s, engineers had suggested the point-loaded test to measure the tensile strength of rock and concrete. Because of its simplicity, this test method is now widely used in rock engineering to detect the tensile strength of rock. However, the preparation of strictly shaped rock specimens is quite difficult. Researchers hope that roughly made specimens, or even irregular ones, can be used directly without affecting the test results. It is therefore important that the shape effect on the stress distributions in different specimens should be investigated systematically.

Sternberg and Rosenthal¹ studied the theoretical problem of an elastic solid sphere subjected to a pair of point loads on the ends of one of its diameters. PingShong *et al.* (in Reference 2) carried out a comparison research on cylindrical specimens using a photoelastic technique as well as an approximate analytical method. Peng (in Reference 2) employed a finite element method to calculate the stress distribution along the loading axis; he suggested that cylindrical specimens with a diameter-to-height ratio larger than unity should be used. In fact, the specimens tested by various workers are usually in the shape of a spheroid. For such cases, some researchers thought that according to Peng's conclusion, it was reasonable to load along the longer principal axis of a spheroidal specimen. At the same time, others argued that it was better to load along the shorter axis of such a specimen. However, their arguments were based only on their experiences from experiments; no theoretical analysis was undertaken. Hence Hean *et al.*³ studied the problem by the photoelastic method. Unfortunately, their research did not lead to any new conclusions on the proper loading direction during tests.

In the present paper we analyse cylindrical and spheroidal specimens with different length ratios of the two principal axes, a/b (see Figure 1), with the aid of an improved adaptive dynamic relaxation method. It is shown that the method used is convenient and efficient. Numerical results

reveal that the better loading direction is along the shorter principal axis of a spheroidal specimen. In addition, we suggest an empirical formula for engineers to evaluate the tensile strength of test materials.

2. FORMULAE AND ALGORITHM

2.1. The basic equations

It is assumed that the specimen material is isotropic and its deformation is elastic, obeying Hooke's law. We investigate the deformation of spheroidal specimens subjected to a pair of compressive point loads on their principal axes, and of circular cylinders loaded on their axisymmetric axes, as shown in Figure 1. We examine the axisymmetric problem such that we have corresponding equilibrium equations in cylindrical co-ordinates without body forces:

$$\begin{aligned}\partial\sigma_r/\partial r + \partial\tau_{rz}/\partial z + (\sigma_r - \sigma_\phi)/r &= 0 \\ \partial\sigma_z/\partial z + \partial\tau_{rz}/\partial r + \tau_{rz}/r &= 0\end{aligned}\quad (1)$$

Consequently the constitutive equations can be written as

$$\begin{aligned}E\varepsilon_r &= \sigma_r - v(\sigma_\phi + \sigma_z) \\ E\varepsilon_\phi &= \sigma_\phi - v(\sigma_z + \sigma_r) \\ E\varepsilon_z &= \sigma_z - v(\sigma_r + \sigma_\phi) \\ E\gamma_{rz} &= 2(1 + v)\tau_{rz}\end{aligned}\quad (2)$$

and the relationships between strains and displacements are expressed as

$$\begin{aligned}\varepsilon_r &= \partial u / \partial r, & \varepsilon_\phi &= u / r, & \varepsilon_z &= \partial w / \partial z \\ \gamma_{rz} &= \partial u / \partial z + \partial w / \partial r\end{aligned}\quad (3)$$

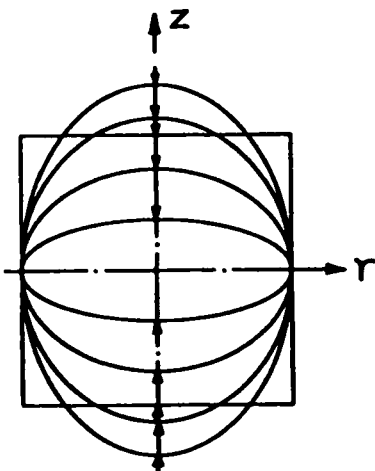


Figure 1. Meridional plane view of spheroidal specimens and a cylindrical specimen

The substitution of equations (2) and (3) into (1) yields

$$\begin{aligned} (\partial\Theta/\partial r)/(1-2v) + \nabla^2 u - u/r^2 &= 0 \\ (\partial\Theta/\partial z)/(1-2v) + \nabla^2 w &= 0 \end{aligned} \quad (4)$$

In the above equations, u and w are displacement components in the r - and z -directions respectively, v is Poisson's ratio and

$$\Theta = \partial w / \partial z + \partial u / \partial r + u / r \quad (5)$$

$$\nabla^2 = \partial^2 / \partial r^2 + \partial / (r \partial r) + \partial^2 / \partial z^2 \quad (6)$$

Equations (4) are what we shall solve later in the paper.

2.2. The algorithm for the present problem

Several numerical methods can be used to solve the present problem. The finite element method (FEM) is a popular one. However, it should be pointed out that a huge computer memory space is needed for solving problems with serious local stress concentration, where a large number of elements are required. For example, the solution of deformable bodies subjected to concentrated loads requires a large computer or the development of complicated programming techniques.

In this paper an improved dynamic relaxation method (IDRM) is applied to solve the basic equations (4). The method has been proved to be powerful for solving the elastic-plastic bending and buckling of plates.^{4,5} It is based on the fact that the static solution of a system is the steady state part of the transient response to step loading. By introducing a central difference scheme with respect to time, the iteration procedure of the method is completely explicit so that only a small computer memory space is needed and all calculations can be carried out by a micro-computer. It has been shown^{5,6} that a better convergence rate and numerical stability will be obtained if the IDRM is combined with the finite difference method (FDM) rather than the FEM. Moreover, with our deduced equations (4), the FDM can easily be applied with respect to spatial co-ordinates r and z .

Accordingly, we first change equations (4) into the corresponding dynamic equations

$$\begin{aligned} m_u u_{tt} + c_u u_t + (\partial\Theta/\partial r)/(1-2v) + \nabla^2 u - u/r^2 &= 0 \\ m_w w_{tt} + c_w w_t + (\partial\Theta/\partial z)/(1-2v) + \nabla^2 w &= 0 \end{aligned} \quad (7)$$

where the subscript ' t ' stands for differentiation with respect to time t , m_u and m_w are mass factors and c_u and c_w are damping factors. It should be noted here that we are now not interested in the dynamic process of the system; therefore time t can be considered as pseudo-time and the mass and damping factors can be fictitiously chosen so that the static solution is obtained in the minimum number of iteration steps and the computation becomes as simple as possible. Keeping these points in mind and choosing $c_u = cm_u$ and $c_w = cm_w$, we obtain explicit formulae for the solutions of u and w when the central difference scheme with respect to t is applied:

$$\begin{aligned} u_{tt}^{k+1/2} &= [(2 - t^k c^k) u_{tt}^{k-1/2} + 2t^k r_u / m_u] / (2 + t^k c^k) \\ w_{tt}^{k+1/2} &= [(2 - t^k c^k) w_{tt}^{k-1/2} + 2t^k r_w / m_w] / (2 + t^k c^k) \\ u^{k+1} &= u^k + t^{k+1} u_{tt}^{k+1/2} \\ w^{k+1} &= w^k + t^{k+1} w_{tt}^{k+1/2} \end{aligned} \quad (8)$$

Here t^k is the time increment at the k th iteration and

$$\begin{aligned} r_u &= -(\partial \Theta^k / \partial r) / (1 - 2\nu) - \nabla^2 u^k + u^k / r^2 \\ r_w &= -(\partial \Theta^k / \partial z) / (1 - 2\nu) - \nabla^2 w^k \end{aligned} \quad (9)$$

while c^k is calculated from Rayleigh's quotient as

$$c^k = 2[\mathbf{X}^T \mathbf{r} / (\mathbf{X}^T \mathbf{M} \mathbf{X})]^{1/2} \quad (10)$$

where

$$\mathbf{X}^T = (u^k, w^k), \quad \mathbf{r}^T = (r_u, r_w), \quad \mathbf{M} = \begin{pmatrix} m_u & 0 \\ 0 & m_w \end{pmatrix} \quad (11)$$

The elements of \mathbf{M} are determined by the Gerschgorin theorem on the limit circle of eigenvalues as

$$m_u \geq 0.25(t^k)^2 \sum_j |k_{ju}|, \quad m_w \geq 0.25(t^k)^2 \sum_j |k_{jw}| \quad (j = u, w) \quad (12)$$

where k_{ij} ($i = u, w$; $j = u, w$) are the elements of the matrix

$$\mathbf{K} = \partial \mathbf{r} / \partial \mathbf{X} \quad (13)$$

More details can be found in References 4 and 5.

For the reasons stated above, we now replace equations (5) and (9) by their corresponding finite difference versions. Assuming that the position of a node in the plane of the finite difference scheme is described by a pair of subscripts (i, j) , where i indicates the position of the node in the r -direction and j its position in the z -direction, as shown in Figure 2, we get

$$\begin{aligned} r_{u(i,j)} &= -0.5(\Theta_{i+1,j} - \Theta_{i-1,j}) / [(1 - 2\nu)\Delta r] - (\nabla^2 u)_{i,j} + u_{i,j} / r_{i,j}^2, \\ r_{w(i,j)} &= -0.5(\Theta_{i,j+1} - \Theta_{i,j-1}) / [(1 - 2\nu)\Delta z] - (\nabla^2 w)_{i,j} \\ \Theta_{i,j} &= 0.5[(w_{i,j+1} - w_{i,j-1}) / \Delta z + (u_{i+1,j} - u_{i-1,j}) / \Delta r] + u_{i,j} / r_{i,j}, \end{aligned}$$

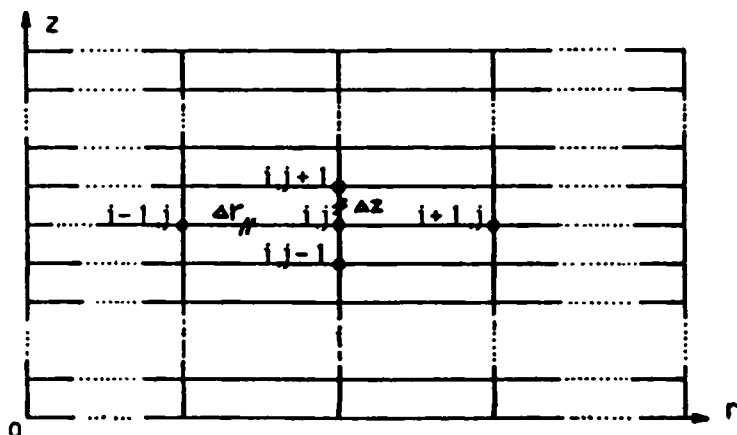


Figure 2. FDM mesh in the r - z plane

where

$$(\nabla^2 \mathbf{X})_{i,j} = (\mathbf{X}_{i+1,j} - 2\mathbf{X}_{i,j} + \mathbf{X}_{i-1,j})/(\Delta r)^2 + 0.5(\mathbf{X}_{i+1,j} - \mathbf{X}_{i-1,j})/r\Delta r + (\mathbf{X}_{i,j+1} - 2\mathbf{X}_{i,j} + \mathbf{X}_{i,j-1})/(\Delta z)^2$$

and Δr and Δz are the lengths of the finite difference mesh in the r - and z -directions respectively.

Therefore the whole algorithm of the IDRM combined with the FDM for the present problem can conveniently be written as follows.

1. Give initial values of \mathbf{X}^0 , \mathbf{X}_r^0 and c^0 .
2. Compute \mathbf{M} and \mathbf{r} from equations (12) and (9).
3. If $\mathbf{r} \approx 0$, stop; otherwise continue.
4. Calculate $\mathbf{X}_r^{k+1/2}$, c^k and \mathbf{X}^{k+1} from equations (8) and (10).
5. Exert boundary conditions (include load and displacement conditions at boundaries).
6. $k = k + 1$ and return to step 2.

Reference 5 gave an efficient method to yield initial values required in step 1 and some other convergence criteria to stop the iteration.

3. NUMERICAL RESULTS AND DISCUSSION

Firstly, to examine the accuracy of the present method, two typical problems are solved and the results are compared with available analytical, numerical and experimental data. In Table I the results obtained using the present method are compared with PingSong's analytical results for an elastic sphere. The sphere is subjected to a pair of locally uniformly distributed pressures over the area with 5° of central angle, as shown in Figure 3. Figure 4(a) presents the results for an elastic circular cylinder and Figure 4(b) for a spheroid subjected to a pair of point loads. In Figure 4 the data obtained from the photoelastic method³ and the finite element method⁷ are also given for comparison purposes. All of these show that the new method is efficient and leads to very accurate predictions.

A set of spheroidal specimens of the same size with one principal axis and a circular cylindrical specimen are then investigated systematically. Two compressive point loads are exerted along the principal axis coinciding with the z -axis as shown in Figure 1. Typical results are given in Figure

Table I. Results for an elastic sphere ($\sigma = P/\pi R^2$, $v=0.3$)

| r/R | z/R | σ_r/σ | | σ_z/σ | |
|-------|-------|-------------------|-----------------------|-------------------|-----------------------|
| | | Present | PingSong ² | Present | PingSong ² |
| 0.0 | 0.5 | 0.15 | 0.15 | -1.42 | -1.43 |
| 0.0 | 0.4 | 0.26 | 0.26 | -1.77 | -1.78 |
| 0.0 | 0.3 | 0.38 | 0.38 | -2.14 | -2.13 |
| 0.0 | 0.2 | 0.50 | 0.50 | -2.45 | -2.13 |
| 0.0 | 0.1 | 0.58 | 0.58 | -2.65 | -2.65 |
| 0.0 | 0.0 | 0.61 | 0.61 | -2.73 | -2.73 |
| 0.1 | 0.0 | 0.62 | 0.62 | -2.81 | -2.81 |
| 0.2 | 0.0 | 0.63 | 0.63 | -3.09 | -3.12 |
| 0.3 | 0.0 | 0.66 | 0.66 | -3.60 | -3.68 |
| 0.4 | 0.0 | 0.71 | 0.71 | -4.49 | -4.49 |
| 0.5 | 0.0 | 0.76 | 0.79 | -6.00 | -6.32 |

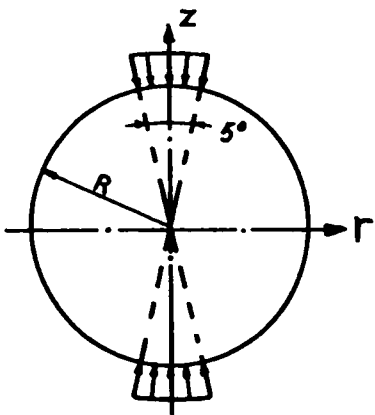


Figure 3. Meridional plane view of a sphere subjected to local pressure

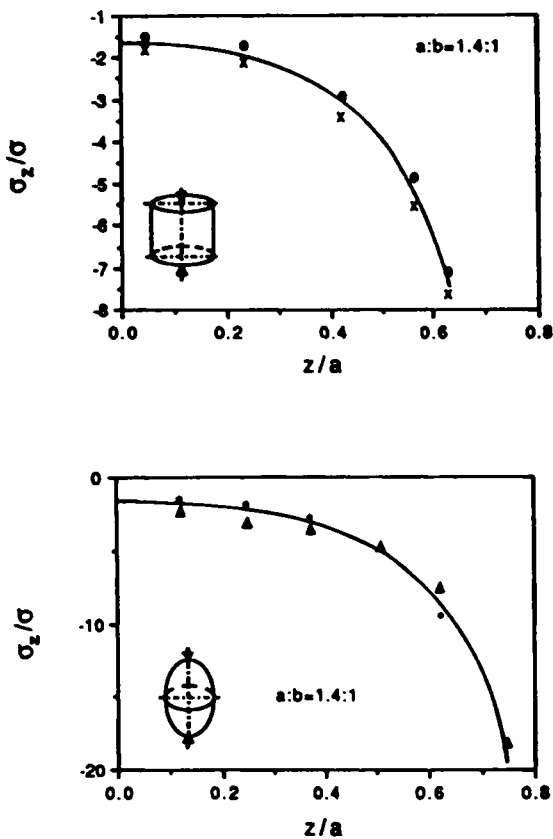


Figure 4. Comparison between experimental and FEM results ($\sigma = P/nb^2$, $v = 0.3$): (a) ---, present results for a circular cylinder with $a/b = 1.4/1$; \times , experimental results; ●, FEM results; (b) —, present results for a spheroid with $a/b = 1.4/1$; ▲, experimental results; *, FEM results

5. Poisson's ratio is taken to be 0.26 throughout the calculations according to the data provided by Reference 2. As is usual in engineering practice, negative stresses and negative tractions in the theory of elasticity are termed compressive in this paper.

It is evident that along the axisymmetric axis of a specimen the shear stress τ_{rz} is zero and that maximum values of $|\sigma_r|$ and $|\sigma_z|$ appear on the loading axis (where $\sigma_r = \sigma_z$). As with the results shown in Figure 4, compressive vertical stress σ_z along the loading axis is observed. However, the distribution of radial stress σ_r is very different from the former (see Figure 5). It is positive in a

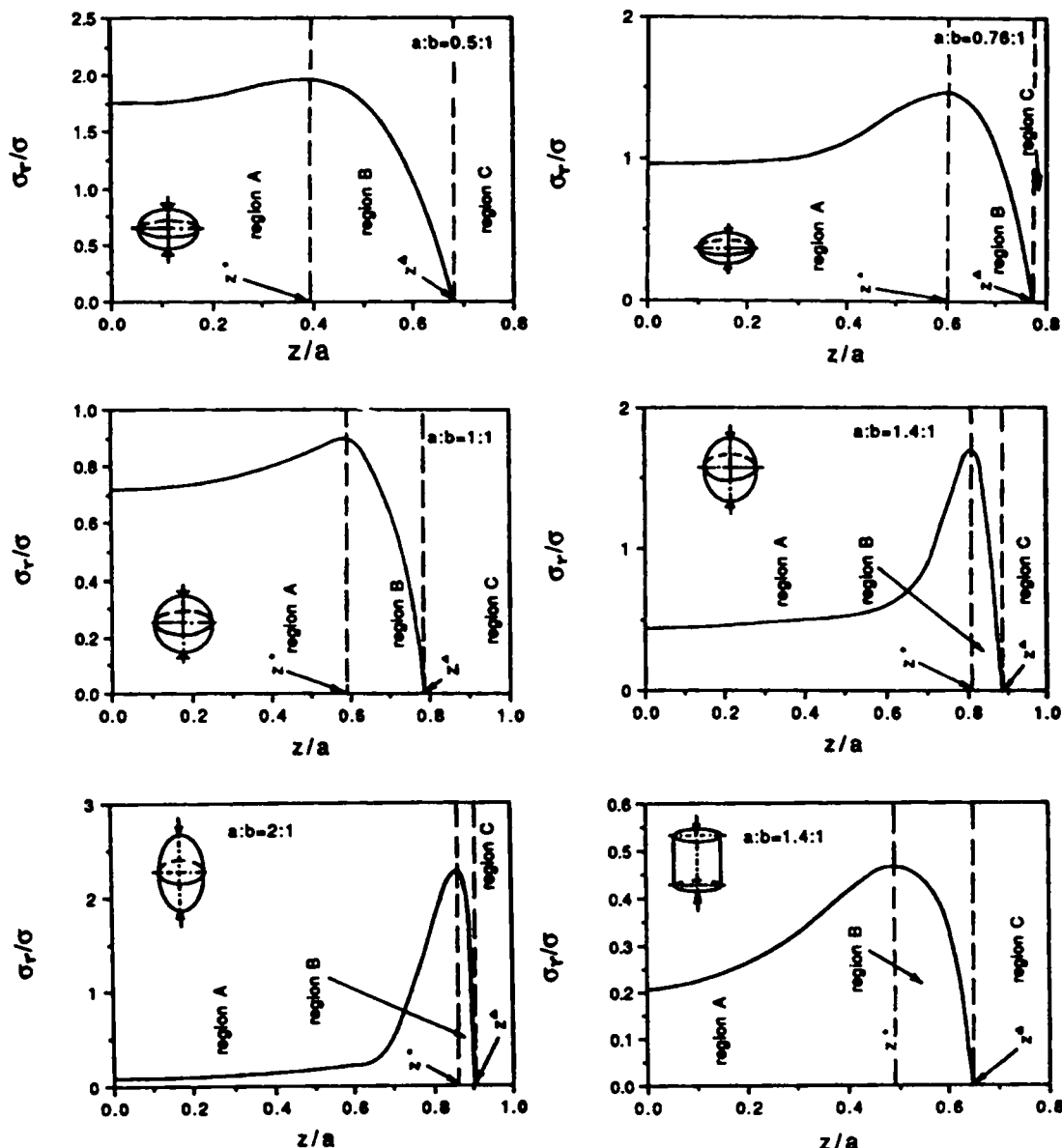


Figure 5. Distributions of radial stresses ($\sigma = P/\pi b^2$, $\nu = 0.26$)

relatively wide region near $z=0$ but changes sharply to negative close to the ends of the specimen. Such a steep variation is due to the stress singularity at the ends of the specimen, where concentrated loads are exerted. For the sake of convenience, let us introduce the following definitions for the distribution of σ_r along the *loading axis* (i.e. the vertical axisymmetric axis of the specimen):

region A—from $z/a=0$ to $z^*=z/a|_{\sigma_r=0}$, $\sigma_r>0$ in this region

region B—from z^* to $z^\Delta=z/a|_{\sigma_r=0}$, $\sigma_r\geq 0$ in this region

region C—from z^Δ to $z/a=1$, $\sigma_r<0$ in this region.

Obviously, region C is a narrow one; inside this region a specimen undergoes compressive stresses in all directions. Hence, if we think that a failure criterion of maximum tensile stress is suitable to evaluate the collapse strength of brittle materials,² the specimen could not break in this region, since the compressive strength of these materials is much higher than their tensile one. Moreover, it shows that as the ratio a/b increases, the ratio (length of region C)/ a becomes smaller and the stress variation from positive to negative in regions B and C becomes steeper. There is an interesting phenomenon associated with the variation of the maximum value of σ_r . It decreases as a/b increases from 0.5 but increases after $a/b=1$. It is worth noting that σ_r varies quite smoothly inside regions A and B since a/b is less than unity. However, a peak appears after $a/b>1$. For such a picture of stress distribution, our applied failure criterion indicates that a point-loaded specimen will break first inside a region on the loading axis just underneath the loading point, but not at the loading point. This is quite consistent with experimental observations.

Obviously, a smoothly distributed tensile stress σ_r is favourable to the evaluation of the strength of a specimen, since a stress peak will bring additional complex problems. Hence this suggests that specimens with $a/b<1$ are proper ones in practice. It then follows that a better loading direction in point-loaded tests is to load along the shorter principal axis. In fact, in terms of the convenience of loading during tests, it is also a better way.

According to the reasoning for the evaluation of tensile strength stated above, an empirical formula can be obtained to relate the maximum external point load P_{\max} and the tensile strength of the specimen, σ_{st} , from the present numerical analysis, i.e.

$$\sigma_{st}/\sigma = \alpha \quad (14)$$

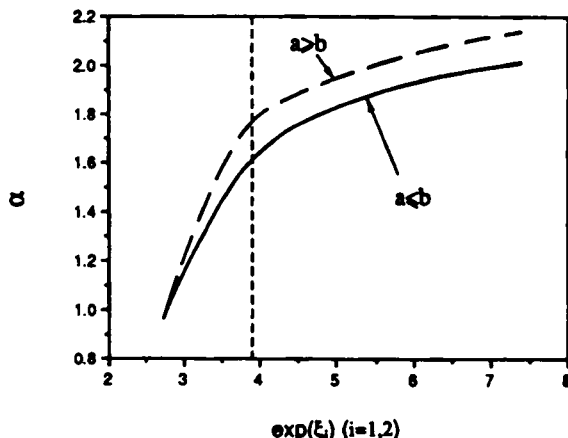
Here $\sigma = P_{\max}/\pi b^2$ is the maximum average stress on section $z=0$; α is a function of the ratio a/b and can be expressed approximately as

$$\alpha = \begin{cases} -4.664 + 3.8235 \exp(\xi_1) - 0.8593 \exp(2\xi_1) + 0.0879 \exp(3\xi_1) - 0.0034 \exp(4\xi_1) & \text{when } a/b \leq 1 \\ -8.4209 + 6.8499 \exp(\xi_2) - 1.7116 \exp(2\xi_2) + 0.1914 \exp(3\xi_2) - 0.0080 \exp(4\xi_2) & \text{when } a/b > 1 \end{cases}$$

by fitting the calculated results, where $\xi_1 = b/a$ and $\xi_2 = a/b$. Alternatively, α can be obtained from Figure 6. It is noted that formula (14) indicates that specimens with $a/b \approx 1$ are not appropriate if we prefer to test at lower P_{\max} for a given material (and hence σ_{st} is a constant), since α reaches its minimum at $a/b=1$. Moreover, Figure 6 shows that α has a high rate of change with respect to ξ_i ($i=1, 2$) when $\exp(\xi_i)$ is less than 3.8. It follows that to get a more accurate estimate of σ_{st} , one is better to choose specimens with $b \geq 1.3a$.

The stress distributions of circular cylindrical specimens shown in Figures 4 and 5 are very similar to those of spheroidal ones with a/b less than unity. This indicates that cylindrical specimens can also be used properly in practice.

Finally, it should be pointed out that the present method also yields reasonable distributions of stresses in region C. This indicates that the method can trace problems with high stress concentrations well.

Figure 6. Variation of α

4. CONCLUDING REMARKS

The present analysis leads to the following conclusions.

1. For a spheroidal specimen with $a/b < 1$, the best loading direction is along the shorter principal axis if the failure criterion of maximum tensile stress is applied. This is also true for irregular specimens with geometries similar to that of a spheroid.
2. The new method described is convenient and efficient. The IDRM is also powerful enough to solve problems with higher stress concentrations.
3. The empirical formula (14) is helpful for evaluating the tensile strength.

Further studies are worthwhile on the effects of transverse isotropy, anisotropy, plasticity and the real boundary traction distributions at the ends of a specimen.

APPENDIX: NOTATION

| | |
|------------|---|
| a | length of vertical semi-axis of a spheroidal specimen or half-height of a circular cylinder |
| b | length of horizontal semi-axis of a spheroidal specimen or radius of a circular cylinder |
| c_u, c_w | transient damping factors in the r - and z -directions respectively, defined by equations (7) |
| E | Young's modulus |
| K | rigidity matrix, defined by equation (13) |
| m_u, m_w | transient mass factors in the r - and z -directions respectively, defined by equations (7) |
| M | defined by equation (11) |
| p | compressive point load |
| r | radial co-ordinate |
| r | defined by equation (11) |
| R | radius of a spherical specimen, as shown in Figure 3 |
| t | pseudo-time |
| u | radial displacement, in the r -direction |

| | |
|--|--|
| w | vertical displacement, in the z-direction |
| X | defined by equation (11) |
| z | vertical co-ordinate |
| γ_{rz} | shear strain |
| $\varepsilon_r, \varepsilon_\phi, \varepsilon_z$ | strain components in the r-, ϕ - and z-directions respectively |
| Θ | defined by equation (5) |
| v | Poisson's ratio |
| σ | average stress, defined by Table I, Figures 4 and 5 or equation (14) |
| $\sigma_r, \sigma_\phi, \sigma_z$ | stress components in the r-, ϕ - and z-directions respectively |
| τ_{rz} | shear stress |
| φ | circumferential co-ordinate |

Superscript

k at the kth iteration step

Subscripts

't differentiation with respect to time
 i, j node number in the plane of the finite difference scheme, defined by Figure 2

REFERENCES

1. E. Sternberg and F. Rosenthal, 'The elastic sphere under concentrated loads', *Trans. ASME, J. Appl. Mech.*, **19**, 413-423 (1952).
2. Chendu Institute of Geology, Proc, *Point-Loaded Test of Rock*, Chinese Geological Press, Chendu, 1979.
3. Hean Futian, Xiao Yongqian and Huang Jiying, 'Analysis of stress distributions of irregular specimens by 3-D photoelastic technique', *Chinese J. Hydrol. Eng. Geol.*, **5**, 101-105 (1981).
4. L. C. Zhang, 'An improved dynamic relaxation solution of circular elastic plates under arbitrary axisymmetric external loads', (in Chinese, with English summary), *J. Zhejiang Univ.*, **23**, 714-721 (1989).
5. L. C. Zhang, T. X. Yu and R. Wang, 'Investigation of sheet metal forming by bending, Parts I-IV', *Int. J. Mech. Sci.*, **31**, 285-348 (1989).
6. P. Underwood, 'Dynamic relaxation', in T. Belytschko and T. J. R. Hughes (eds), *Computational Methods for Transient Analysis*, Elsevier, Amsterdam, 1983.
7. L. C. Zhang and Ding Haojiang, 'FEM analysis of axisymmetric bodies subjected to arbitrary distributed loads', *Technical Report*, Department of Mechanics, Zhejiang University, 1981.